Analysis of Neutron Damage in High-Temperature Silicon Carbide JFETs

F. Barry McLean, James M. McGarrity, Charles J. Scozzie,
C. Wesley Tipton, and W. Merle DeLancey

US Army Research Laboratory
2800 Powder Mill Road
Adelphi, Md 20783

Abstract

Neutron-induced displacement damage effects in n-channel, depletion-mode junction-field-effect transistors (JFETs) fabricated on 6H-silicon carbide are reported as a function of temperature from room temperature (RT) to 300°C. The data are analyzed in terms of a refined model that folds in recently reported information on the two-level ionization energy structure of the nitrogen donors. A value of 5 ± 1 cm^{-3} per n/cm^2 is obtained for the deep-level defect introduction rate induced by the neutron irradiation. Due to partial ionization of the donor atoms at RT, the carrier removal rate is a function of temperature, varying from 3.5 cm^{-1} at RT to 4.75 cm^{-1} at 300°C. The relative neutron effect on carrier mobility varies with temperature approximately as $T^{-7/2}$, dropping by an order of magnitude at 300°C compared with the RT effect. The results offer further support for the use of SiC devices in applications which combine high-temperature and severe radiation environments, where the use of Si and GaAs technologies is limited.

I. Introduction

Silicon carbide is an emerging wide-bandgap (2.9 eV in 6H-SiC) semiconductor technology, which has the potential to meet the operating requirements of electronics for commercial and space nuclear power applications. Typical environmental requirements include high-temperature operation (400–500°C), high radiation tolerance (100 Mrads and 1×10^{16} n/cm^2), and a useful lifetime of 7 to 10 years. The use of high-temperature radiation-hard electronics would simplify the design of nuclear power systems. For example, radiation-resistant, high-temperature multiplexers could be used inside the pressure vessels on commercial nuclear power reactors, which would reduce the number of penetrations of the pressure vessel required to bring out signals for reactor monitoring and control. It would also enable installation of additional sensors for monitoring the status of the reactor core and structural elements. Similar simplifications could be made in the design of space nuclear power systems such as the SP-100 thermoelectric power generator and the TOPAZ thermonic nuclear power source. Operating the electronics at a high temperature would save significant weight by reducing the cooling requirements for the electronics. (Si electronics will operate reliably for 10 years only if the operating temperature is maintained at less than 100°C.) Also, high-temperature radiation-resistant electronics could be placed closer to the nuclear power source, thereby reducing the requirement to run signal and control cables over long distances to a control module where the electronics is operated at much lower temperature and with much less radiation exposure. Thus, in addition to saving weight the system complexity can be reduced, which usually translates into an increased system reliability. This paper is part of an ongoing study by our group to validate the promise of SiC for such applications. The goal of our research is ultimately to demonstrate that high-temperature radiation-hardened circuits can be designed and fabricated to meet these kinds of needs.

At this conference in 1992, we presented the results of a neutron irradiation study on buried gate, n-channel, junction field-effect transistors (JFETs) fabricated in epitaxial layers grown on 6H-SiC wafers [1]. In that work we used a simple analysis to extract the carrier removal rate and mobility degradation, based on the assumption that the carrier removal rate (a) was the same as the neutron-induced deep-level defect introduction rate (A), which we determined to be 4.5 ± 0.5 cm^{-3} per n/cm^2. The assumption $a = A$ was largely necessitated by the fact that information essential to calculating the change in Fermi potential and hence carrier concentration as a function of neutron fluence (as well as temperature) was lacking—namely, the basic ionization energy structure of the nitrogen (N) donors in 6H-SiC was not yet well established. This information is important in an accurate calculation of a because the N donors are only partially ionized at room temperature in SiC, and the deep trapping levels introduced by the neutron irradiation induce a shift in the Fermi level E_F, which, in turn, affects the ionization probabilities. This information is, of course, also essential to a proper understanding of the temperature dependence of the electrical characteristics of the devices. In late 1992, Suttrop et al [2] published the results of a detailed combined Hall effect and infrared absorption study of n-type 6H-SiC in which they deduced a two-level ionization structure (85 and 125 meV) for the N donors. In a recent study [3] we showed that the temperature dependence of the electrical characteristics of n-channel 6H-SiC JFETs is indeed well described by a carrier concentration calculated using this two-level ionization structure for the N donors along with an inverse power law dependence of carrier mobility on temperature. (The inverse power dependence of mobility on temperature has been reported generally in the literature, usually based on Hall measurements [4–9].)

The purpose of the present work is twofold: (1) to present additional data on the effects of neutron irradiation on SiC JFETs as a function of temperature from room temperature (RT) to

300°C using new samples of different doping density and lower initial compensation than used in our earlier work [1]; and (2) to present a more complete and accurate analysis of the carrier removal rate and mobility degradation as functions of both neutron fluence and temperature, in which the variations in E_F are accounted for.

In the next section we briefly describe the JFETs used in our present study and then present the experimental results, both the preirradiation temperature characterization and the effects of neutron irradiation for fluences up to 5×10^{15} n/cm^2. In section III we review the two-level ionization energy model for the N donors in n-6H-SiC and briefly review its application to the description of the temperature dependence of the electrical properties. We then discuss the extension of the model to include the neutron effects, in particular, the calculation of carrier removal; and we derive an expression for mobility which points to the strong temperature dependence of the neutron effect on mobility. In section IV we apply the theory to the analysis of the neutron radiation data on our JFETs, focusing in turn on determination of the defect introduction rate, calculation of the carrier removal rate as a function of temperature, and the unfolding of the mobility degradation as a function of temperature and fluence. In section V we discuss some additional points and draw some implications from our work. Then we conclude with the assertion that SiC is indeed a viable technology for high-temperature/high-power electronics that must operate in severe radiation environments.

II. Experimental Results

A. Device Description

The transistors used in this study are buried gate, n-channel, depletion-mode JFETs purchased from CREE Research, Inc. See Fig. 1 for a schematic of the cross-sectional design of the devices. The JFETs were fabricated in epitaxial layers grown on 6H-SiC wafers, packaged on TO-46 headers, and sealed in a nitrogen environment. The channel length, width, and depth of the active channel region of the devices were nominally 5 μm, 1 mm, and 0.32 μm, respectively. The N donor concentration in the channel was 1.2×10^{17} cm^{-3}, as determined at CREE by capacitance-voltage measurements. The bottom (gate-side) p$^+$ epi-layer forming the junction with the channel region was doped to 2×10^{18} cm^{-3} with aluminum acceptors. A thin (≈200 A SiO_2) oxide was thermally grown to passivate the surfaces. The source and drain contacts were deposited nickel, and the bottom gate contact was a deposited Al alloy. The ohmic contacts were annealed at high temperature. The carrier concentration in the channel at RT was 6.2×10^{16} cm^{-3}, and the preirradiation deep acceptor compensation density was 5×10^{15} cm^{-3} [3,9], a relatively low value for SiC. The RT carrier mobility was measured as 320 cm^2/V-s by Hall measurements on n-type epi-layers of comparable doping [9]. To establish the robustness of these devices, 15 of the JFETs were stressed prior to irradiation at 300°C for over 1000 hours [10]. All transistors survived this test with minimal changes (≤5%) in their electrical characteristics.

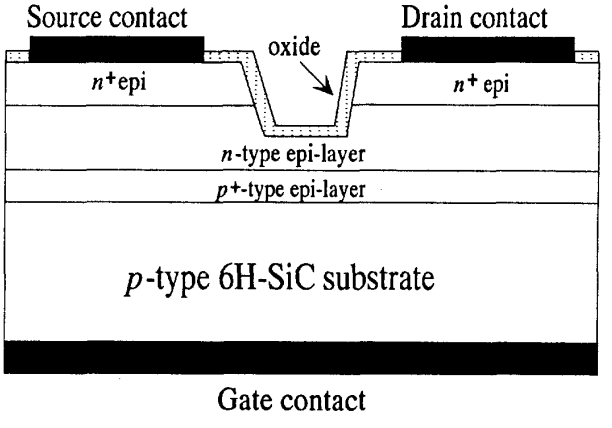

Fig. 1. Cross-sectional view of depletion-mode n-channel SiC JFET.

B. Electrical Characterization

The drain current I_D versus drain-to-source (V_{DS}) and gate (V_G) voltages was measured both before and after neutron irradiation for a series of temperatures between room temperature and 300°C. From these measurements, values for the pinchoff voltage (V_{po}), transconductance (g_m), and saturated drain current (I_{DSS}) were obtained. g_m is defined as the maximum transconductance evaluated at zero gate voltage. V_{po} was extracted from the data using the I_D vs V_G curve, in which the slope of the square root of the curve was extrapolated to the x axis, and the threshold voltage V_T defined as the x intercept. V_T is the externally applied gate voltage required to achieve pinch-off. Then V_{po} is related to V_T via $V_{po} = |V_T| + V_{bi}$, where V_{bi} is the built-in potential at the p^+n gate junction in the channel region. I_{DSS} is defined as the value of the drain current for $V_{DS} = V_T$ at $V_G = 0$.

Figure 2 depicts the temperature dependence of the I_D vs V_{DS} characteristics for a single representative JFET from RT to 400°C. These measurements are for zero gate voltage, where the channel is fully open for a depletion-mode device. The device depicted in Fig. 2 has an RT threshold voltage of 8.65 V, with a corresponding pinchoff voltage of 11.4 V, transconductance of

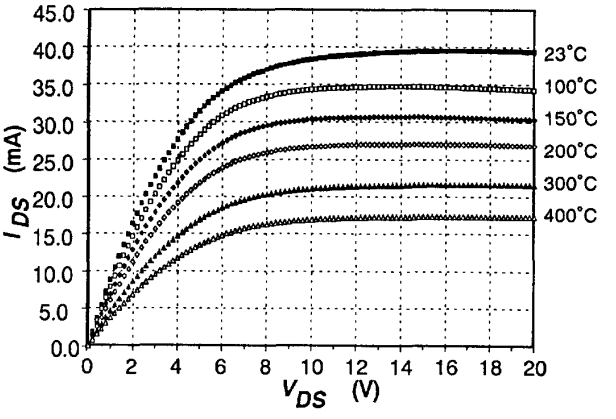

Fig. 2. Measured drain current versus drain-to-source voltage at $V_G = 0$ for series of temperatures.

8.0 mS/mm, and saturated drain current of 38 mA. As the temperature increases, there is a reduction in g_m and the current levels, for example, to g_m = 3.5 mS/mm and I_{DSS} = 17 mA at 400°C, a drop by a factor of a little over two. However, it is clear that good, clean transistor action is obtained throughout the temperature range of Fig. 2. But the keys to the understanding and successful modeling of the electrical properties of the SiC devices are the descriptions of the carrier concentration and mobility as functions of temperature, which we will discuss in section III.

C. Neutron Irradiations

Most of the neutron irradiations were carried out at the Army's Aberdeen Pulsed Reactor Facility (APRF), though we will include a limited amount of neutron irradiation data obtained at the Maryland University Training Reactor (MUTR), mostly as a comparison check of data taken at two different reactor facilities. The dosimetry is better characterized at the APRF (to within 10 percent fast neutron fluence) than at the MUTR (20%); therefore, we put more reliance on analysis of the APRF radiation data. In addition, the gamma dose at the MUTR is almost a factor of ten greater than at the APRF—the gamma to neutron ratio is 2.75×10^{-9} rads(Si)/n/cm^2 at the MUTR and 3.23×10^{-10} rads(Si)/n/cm^2 at the APRF. The irradiations were carried out at both facilities at RT for a series of neutron fluences up to 5×10^{15} cm^{-2}, after which electrical characterizations were done as a function of temperature from RT to 300°C. (However, only RT characterization data after irradiation at the MUTR is utilized in the analysis reported here.) The neutron spectra from the reactors are degraded fission spectra peaked at about 1 MeV. Since fluences expressed in 1 MeV equivalent in SiC were not yet available, we report all fluences in this paper as total fluence of fast neutrons, with energy ≥10 keV.

Representative data of I_D versus V_{DS} at zero gate voltage taken at the APRF are shown in Fig. 3, at room temperature in (a) and at 300°C in (b). (We note these data are for a different device than in Fig. 2.) Included are the preirradiation data and the data after neutron fluences of 1 and 5×10^{15} n/cm^2. Qualitatively, as reported earlier [1], we see a relatively large neutron effect at RT and relatively little neutron effect at 300°C, although the current is reduced by approximately a factor of two by temperature alone. Figure 4 illustrates the neutron irradiation effect (APRF data) on the threshold voltage (4a), transconductance (4b), and saturated drain current (4c), where the data are normalized to the respective preirradiation RT values. Data for a number of fluences and temperatures are included; also, these data represent averages for five devices, with the preirradiation RT average values of –4.78 V, 6.45 mS, and 21.0 mA for V_T, g_m, *and* I_{DSS}, respectively. Again, the decreasing relative neutron effect with increasing temperature is readily apparent.

One interesting effect discernible at RT is the slight enhancement in the device characteristics at low neutron fluence; the device electrical parameters rise slightly with fluence, peaking in the range 1×10^{13} to 1×10^{14} n/cm^2, before dropping off with additional fluence. We attribute this effect to a positive charge buildup in the thin passivation oxide above the channel due to the gamma dose, which is approximately 10 krads(Si) at a neutron

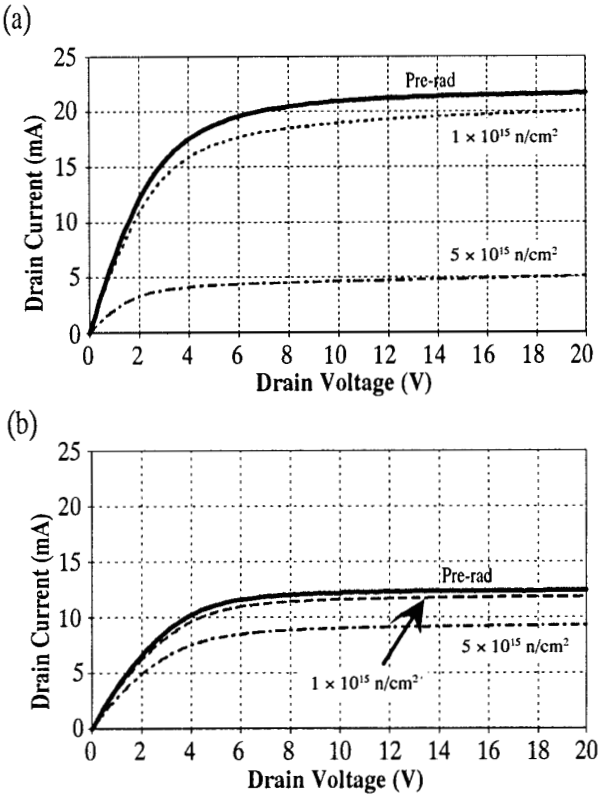

Fig. 3. Measured drain current versus drain-source voltage at zero gate voltage after neutron irradiation at the APRF to several fluences at (a) room temperature and (b) 300°C.

fluence of 3×10^{13} n/cm^2 at the APRF. The positive charge buildup is presumed to result in an accumulation of carrier density in the channel near the SiO_2/SiC interface as well as a small increase in the threshold voltage necessary to pinch off the channel. We assume the oxide charging saturates at around this dose, beyond which the parameters degrade due to the neutron effect. In doing the analysis of the neutron damage, we account for the oxide charging effect essentially by shifting the zero point for the neutron fluence to the point where the maximum in the electrical parameters occurs. For further discussion of this effect, see section V.

In Fig. 5 we show RT in situ I-V data on a single JFET taken at the MUTR. The fluences indicated are nominal values—later analysis of dosimetry indicated the actual fluences were about 10 percent lower. These data, as well as the higher temperature characterizations, are consistent with the data taken at the APRF.

III. Theory

A. JFET Device Equations

In our modeling and analysis we employ the standard, abrupt-junction long-channel JFET device equations. For completeness we give the following expressions which relate the pinchoff voltage, transconductance, and saturated drain current

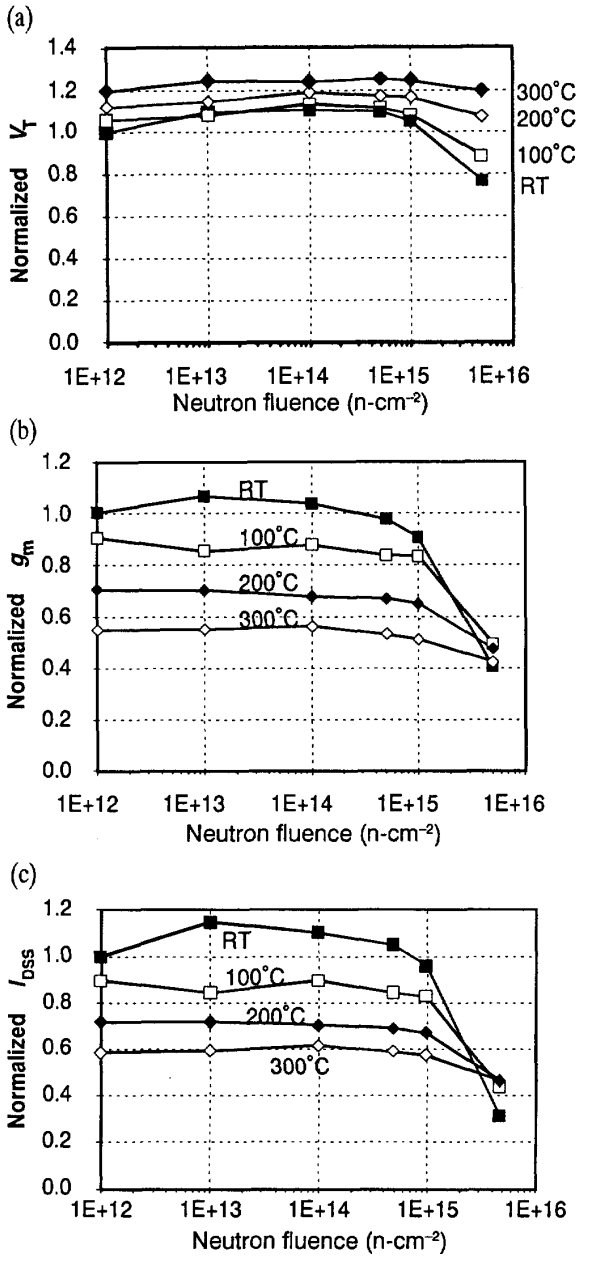

Fig. 4. Normalized average SiC JFET electrical parameters versus neutron fluence (APRF data) at several temperatures showing (a) threshold voltage, (b) transconductance, and (c) saturated drain current at $V_G = 0$. All values are normalized to preirradiation room temperature values.

(at V_G = 0) to the physical dimensions of the device and to the channel doping density ($N_D = 1.2 \times 10^{17}$ cm^{-3}), carrier concentration (n), and carrier mobility (μ) for a uniformly doped channel region [11]:

$$V_{po} = qN_D D^2/2\varepsilon_s \,, \tag{1}$$

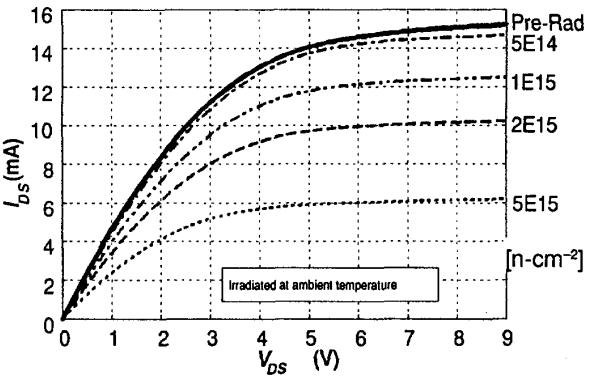

Fig. 5. In situ measurements of drain current versus drain-source voltage at $V_G = 0$ at room temperature for several neutron fluences at the MUTR facility.

$$g_m = qn\mu(DW/L)(1 - x^{1/2}) \,, \tag{2}$$

$$I_{DSS} = (q^2 N_D n\mu/6\varepsilon_s)(D^3 W/L)(1 - 3x + 2x^{3/2}) \,, \tag{3}$$

where $x = V_{bi}/V_{po}$, q is the electronic charge, ε_s is the dielectric constant ($\approx 10\varepsilon_o$ for 6H-SiC), and D, L, W are the channel depth, length, and width, respectively (0.32 μm, 5 μm, and 0.1 cm for our samples). The RT built-in junction potential V_{bi} is 2.75V and decreases by 1.5 mV per degree above room temperature [12], and again we note that V_{po} is related to the measured threshold voltage via $V_{po} = |V_T| + V_{bi}$. We note that for partial ionization—as we have in n-6H-SiC at RT—we must distinguish between the space charge density N_D in the depletion region and the carrier concentration n in the quasi-neutral channel region, as discussed previously in more detail [1].

B. Two-Level Donor Ionization Model

Figure 6 illustrates the basic schematic model we use to calculate the carrier concentration n as a function of temperature both before and after neutron irradiation. We have space here to just briefly indicate the procedure. The two-level N donor ionization scheme inferred by Suttrop et al [2] is indicated in the figure, as well as a broad band of deep-level acceptor-like traps (with unknown energies). The lower donor level of 85 meV is associated with N donors located in sites having local hexagonal geometry and the larger ionization energy of 125 meV with N donors in cubic sites, with a relative concentration ratio of the two geometric sites, typically 1:2, respectively. The deep-level compensation concentration (N_K) is assumed to be temperature independent. (The placement of the Fermi level E_F in Fig. 6 is schematically appropriate for a temperature somewhat greater than RT prior to irradiation. Also, the bandgap energy is actually temperature dependent; the indicated value of 2.9 eV is an appropriate average value over the temperature range from RT to 400°C [6].) We previously [3] calculated $n(T)$ using this energy structure, along with the basic equilibrium condition of charge neutrality in the channel (net negative charge density equals net positive charge density),

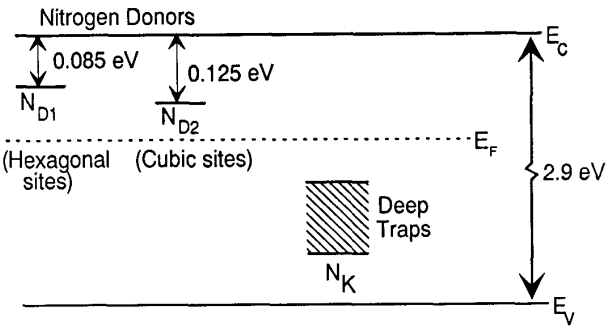

Fig. 6. Schematic energy band diagram for n-type, 6H-SiC showing N donor ionization energies and deep-level compensation traps.

$$n + N_K = N_{D1}^{+} + N_{D2}^{+} , \tag{4}$$

where the ionization of the impurity levels is determined using Fermi-Dirac statistics:

$$N_{Di}^{+} = N_{Di}[1 + (gn/N_c)exp(E_{di}/kT)]^{-1}. \tag{5}$$

We used the standard expression [11] for n in terms of the Fermi energy, $n = N_c exp[-(E_c - E_F)/kT]$, to eliminate E_F and thereby cast Eq. (4) into an equation with the single unknown quantity $n(T)$. In these expressions $g = 2$ is the donor degeneracy factor, k the Boltzmann constant, E_{di} are the ionization energies of the two donor states (85 and 125 meV as indicated in Fig. 6), and N_c is the effective density of states in the conduction band. We calculated $N_c = 2M(2\pi m^* kT/h^2)^{3/2}$ [11] using $0.3m_o$ as the effective density-of-states mass m^* [2], where m_o is the free electron mass and h is Planck's constant, and assuming three equivalent conduction band minima (M) based on recent band structure calculations [13,14]. We obtained 1.25×10^{19} cm^{-3} as the RT effective density of states, which then scales as $T^{3/2}$ with temperature. Based on Suttrop et al [2] we assumed $N_D = N_{D1} + N_{D2}$, where $N_{D2} \approx 2N_{D1}$, and we also note that the total donor density N_D to be used here is the sum of the effective, or measured, space charge density (1.2×10^{17} cm^{-3}) and the compensation density N_K. (In the device equations, Eqs. (1) and (3), it is the effective donor density that should be used, $N_D^{eff} = N_D - N_K$.) Finally, we ascertained the preirradiation value of the compensation density by fitting Eqs. (1)–(3) to the room temperature electrical measurements, thereby determining a value for n at RT (0.62×10^{17} cm^{-3}), and then solving Eq. (4) for N_K. We obtained a compensation value of 5×10^{15} cm^{-3}, which also is in agreement with the value found by Schaffer et al [9] from fitting the Hall data on epi-layers of comparable doping.

Figure 7(a) shows the result of applying this procedure to the calculation of $n(T)$ for our devices before neutron irradiation [3]. Note that the carrier density is only about half activated at RT, and that full ionization is not achieved until the temperature exceeds about 700 K. This is in contrast to the usual situation in Si or GaAs where the carrier concentration is fully activated at RT. We used the $n(T)$ shown in Fig.7(a), along with an inverse square dependence of mobility μ on temperature [3,9] to calculate the electrical characteristics as a function of temperature. (In ref. 3 we ascertained the inverse square power law dependence of μ on temperature by a best-fit analysis of the measured saturated drain current as a function of temperature. This analysis agreed very closely with the Hall mobility measurements as a function of temperature made on comparably doped epi-layers as reported by Schaffer et al [9], which is shown in Fig. 7(b).) Figure 8, which is also taken from ref. 3, compares the calculated and measured saturated drain current I_{DSS} as a function of temperature, and illustrates the good agreement between the model calculations and experimental data for temperatures up to 400°C. There is some deviation between the measured and calculated values in the temperature range above 300°C. However, we observed a slight increase in pinchoff voltage at and above 300°C of about 5 percent. We postulated that this is due to ionization of deeper donor levels or traps at the higher temperatures, which is not

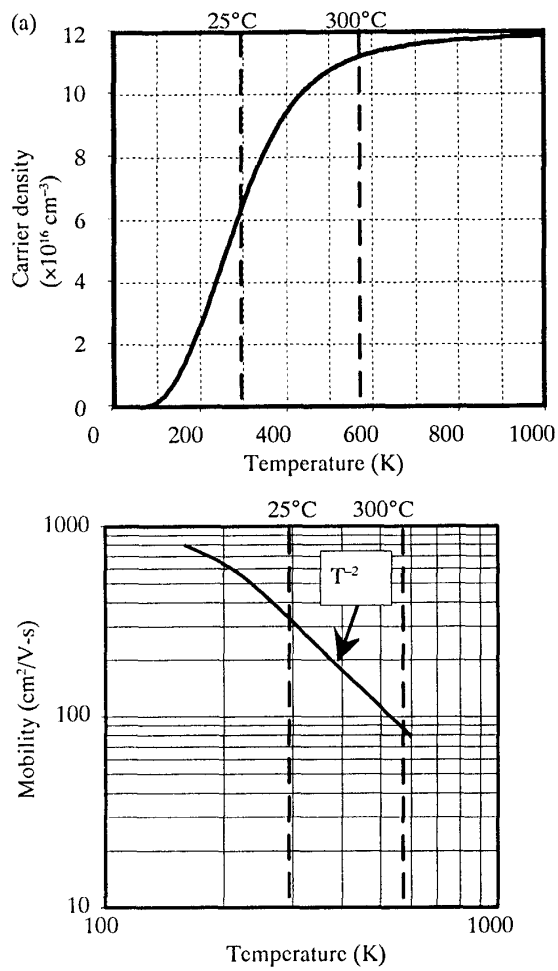

Fig. 7. Temperature dependence of (a) carrier concentration calculated based on two-level donor ionization structure (from ref. 3), and (b) carrier mobility from Hall measurements (after ref. 9).

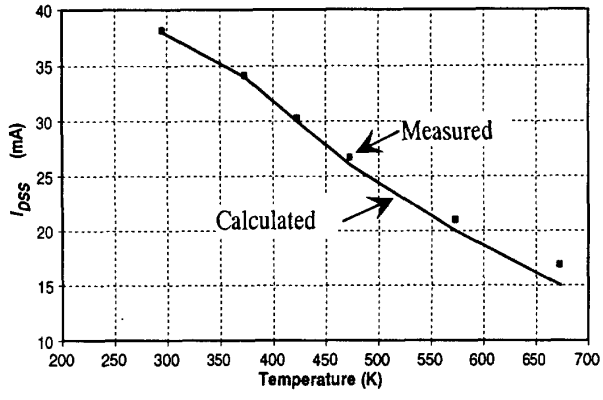

Fig. 8. Comparison of preirradiation calculated and measured saturated drain current versus temperature for $V_G = 0$ (from ref. 3).

included in the model. If we adjust the calculation to account for the increased charge density indicated by the pinchoff voltage, we obtain much closer agreement between the calculated and measured current values at the higher temperatures. In any case the quite acceptable agreement between calculated and measured I_{DSS} indicated in Fig. 8 gives us confidence in applying the two-level donor ionization model to analysis of the effects of neutron irradiation.

C. Effect of Neutron Irradiation

We assume that the primary result of neutron irradiation is to induce displacement damage which introduces deep-level traps (acceptor-like for n-type material) within the bandgap [15,16]. We assume these additional traps effectively can be treated as an increase in the compensation density,

$$N_K = N_K^o + A\phi \tag{6}$$

where A is the defect introduction rate assumed to be constant with neutron fluence ϕ. We also assume that the neutron-induced traps are sufficiently deep that they remain occupied by electrons at all temperatures of concern in the quasi-neutral channel region. (We do not assume that they remain filled in a depletion (space charge) region at high temperature; however, we will assume that the RT measurement of the change in pinchoff voltage after neutron irradiation gives a good measure of the neutron-induced deep-level density, or at least a good lower bound. That this indeed gives a good lower bound to the neutron-induced deep trap density is confirmed by a consistency check at 300°C, where the predominant neutron effect is carrier removal. See discussion in the next section.)

In the channel region there are two primary electrical manifestations of the deep levels: (1) a reduction in the carrier density and (2) a reduction in mobility due to increased scattering of the remaining free carriers with the additional charge centers. We calculate the reduction in n by the same basic procedure described above for $n(T)$ but now use the neutron-induced increase in N_K (Eq. (6)); this procedure takes into account the change in Fermi potential with ϕ under the assumption that the deep levels are fully occupied. The effective carrier removal rate $a(T,\phi)$ is defined by

$$n_\phi = n_o - a\phi \ , \tag{7}$$

where n_O and n_ϕ are the pre- and post-irradiation carrier densities, respectively, and a is in general a function of temperature and fluence, as well as doping density and initial compensation density. However, over the fluence range of the data reported here, the effective (average) carrier removal rate at room temperature drops by only 3% from its low ϕ limit value. Therefore, it is really sufficient to simply give the low fluence expression for a, which we obtain analytically by substituting Eqs. (6) and (7) into the charge neutrality condition, Eq. (4). Then using Eq. (5) and differentiating both sides with respect to ϕ and letting $\phi = 0$, we obtain the result

$$a = A\{1 + (N_D/3)[b_1/(1+b_1 n_o)^2 + 2b_2/(1+b_2 n_o)^2]\}^{-1} \ , \tag{8}$$

where $b_i = (g/N_c)exp(E_{di}/kT)$.

The mobility μ_ϕ after neutron irradiation follows from the basic additive property of scattering rates of carriers in solids and is given by the expression

$$\mu_\phi^{-1} = \mu_o^{-1} + \alpha \Delta N_{sc} \ , \tag{9}$$

where μ_O is the preirradiation mobility, α is a scattering parameter, and ΔN_{SC} is the increase in charged scattering centers responsible for the mobility degradation. ΔN_{SC} is composed of both the neutron-induced charge traps and the increase in ionized N donors resulting from the reduction in E_F with increasing N_K. From the basic charge neutrality equation one finds simply $\Delta N_{SC}(T) = [2A - a(T)]\phi$. The result for μ_ϕ can be put into the form

$$\mu_\phi(T) = \mu_o(T)[1 + \beta(T)\phi]^{-1} \ , \tag{10}$$

where the parameter $\beta(T) = \alpha(T)\mu_o(T)[2A - a(T)]$. But for carriers scattering from charge centers in semiconductors, $\alpha \sim T^{-3/2}$ [11]; and the preirradiation mobility varies as the inverse square power of T [3,9]. Thus μ_ϕ can be written in the form

$$\beta(T) = \beta_o(T_o/T)^{7/2}[2A - a(T)] \ , \tag{11}$$

where β_o is a constant and T_o is a reference temperature, e.g., RT. Thus the simple theory predicts a very strong temperature dependence of the neutron effect on mobility, which as we shall see is borne out by the data.

IV. Analysis of Experimental Data

We now apply the preceding analysis to the neutron irradiation data, discussing in turn the defect introduction rate, carrier removal, and degradation in carrier mobility. As mentioned earlier in section II (see Fig. 4), there is a slight enhancement in the electrical parameters at low fluence levels, primarily at RT, which we attribute to a charge buildup in the passivation oxide above the channel associated with the gamma dose from the reactor. In the following analysis we account for the effect simply

by referencing the fluence values to the fluence at which the peak enhancement occurred in the particular electrical parameter being analyzed.

A. Defect Introduction Rate

We assume that the change in pinchoff voltage with fluence at RT reflects the neutron-induced change in effective doping density in the depletion region, thus yielding an estimate of the defect introduction rate (A). As is evident from a scrutiny of the threshold voltage vs fluence (Fig. 4a), thermal detrapping of the trapped electrons in the neutron-induced deep levels occurs in the depletion layer as the temperature increases, with almost full removal evident at 300°C. Thus the RT change in V_{po} can provide only a lower bound on A, as some detrapping likely occurs from the more shallow neutron-induced levels in the depletion region, even at RT. However, as we shall see below, at 300°C where we expect that carrier removal is the primary cause of the neutron-induced reduction in g_m or I_{DSS}, the carrier removal rate calculated from the A-value as deduced from the RT change in V_{po} is consistent with the data.

Accordingly, in Fig. 9 we plot the experimentally determined RT values of $N_D(1 - V_{p\phi}/V_{po})$ vs ϕ, the slope of which should be a direct measure of A based on Eq. (1)—i.e., the change in effective doping density is just $A\phi$ (using Eq. (6) and $N_D^{eff} = N_D - N_K$). We include data points from our present samples, denoted here by lot B, irradiated at both APRF and MUTR, as well as two data points (at fluences of 1×10^{15} and 1×10^{16} n/cm^2) from our previous work [1] denoted by lot A. The solid line shown is a best-fit straight line to the data. From the slope of the line we determine our estimate of the defect introduction rate of $A = 5 \pm 1.0$ cm^{-3} per neutron per cm^2. This value is somewhat higher than we reported in ref. 1 (4.5 ± 0.5 cm^{-1}), but is still within experimental error. Note, however, that we have doubled the error limits on this basic result, because as we have gained more experience with the JFET devices, the neutron irradiations, and the factors that go into the analysis, we have become more cognizant of the possible errors that may affect the result (the main errors being dosimetry and measurement of preirradiation effective doping density, both being on the order of ±10%). The relatively close data fit shown in Fig. 9 may indicate tighter error limits on A than ±20%, but at this time we are reluctant to ascribe any better accuracy to the result. We note that the A-value we determined for n-6H-SiC is about 40 percent of the value for n-type Si extrapolated to comparable doping density [17]. This is consistent with the higher atomic threshold energy (21.8 eV) for displacement determined for 6H-SiC by Barry et al [18] (using energetic electron bombardment) relative to that for Si (13 eV).

B. Carrier Removal

It is now straightforward to apply the charge neutrality condition (Eq. 4) for the channel region using the two-level ionization energy structure for the N donors and the increased N_K-density (Eq. 6) associated with the value for A determined above to obtain the carrier density as a function of T and ϕ. The results are shown in Fig. 10 for n versus T both before irradiation and after neutron exposure to fluences of 2, 5, and 10×10^{15} n/cm^2 for our present (lot B) devices. In Fig. 11 we show the result

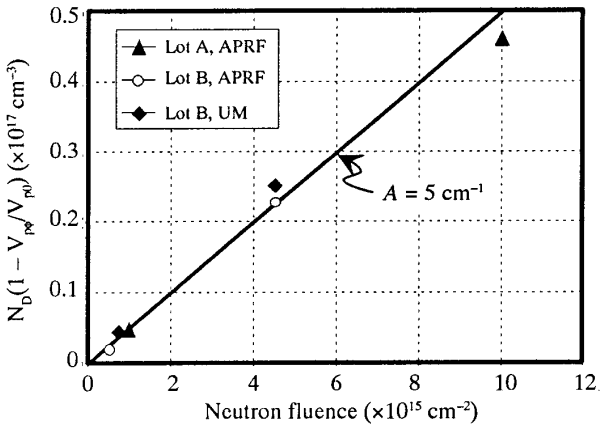

Fig. 9. Determination of defect introduction rate (A) from change in pinchoff voltage at room temperature.

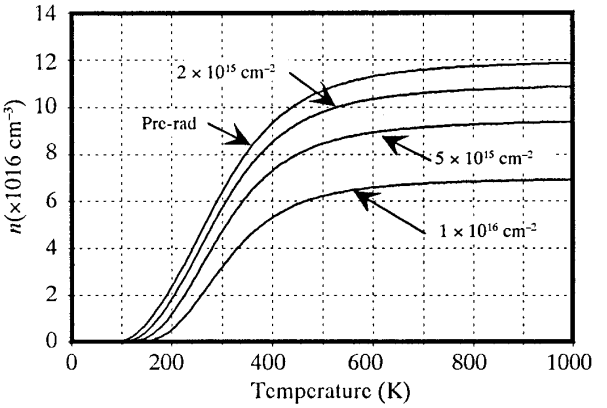

Fig. 10. Calculated carrier concentration versus temperature after neutron irradiation to several fluences.

for the carrier removal rate a in the low fluence limit (Eq. (8)) as a function of temperature from 200 to 700K; note that a varies from 3.5 cm^{-1} at RT (295 K) to 4.75 cm^{-1} at 300°C (573 K), so that only at the higher temperatures does the carrier removal rate approach the defect introduction rate. In effect, in the regime of partial ionization of the donor atoms, the carrier removal due to deep-level trapping is partially offset by increased ionization of the donors (as the Fermi level drops in energy with increased deep trap density). In general, the effective carrier removal rate as defined by Eq. (7) is a function of both temperature and fluence, but as can be discerned from a comparison of figures 10 and 11, for temperatures above RT a differs from its low fluence limit by less than 5% for fluences up to 1×10^{16} cm^{-2}.

For completeness, we show in Fig. 12 some additional calculations of a in the $\phi \rightarrow 0$ limit as a function of temperature for several doping and compensation densities. Curve b is for our present (lot B) devices; curve c is for the lot A devices studied previously [1], which have a relatively high compensation density (25% of the effective doping density); and curves a and d are for hypothetical devices of significantly lower (5×10^{16} cm^{-3}) and higher (5×10^{17} cm^{-3}) doping densities, respectively, where

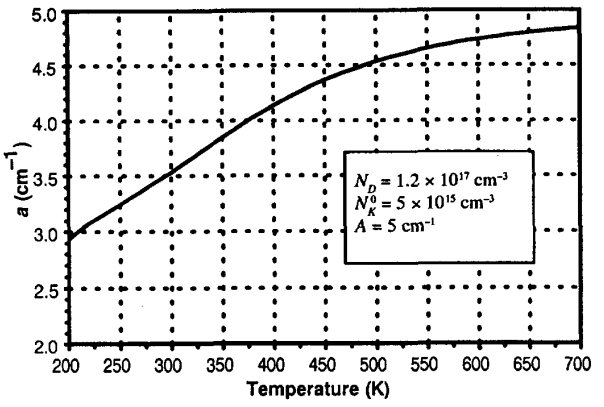

Fig. 11. Carrier removal rate as a function of temperature in the low fluence limit.

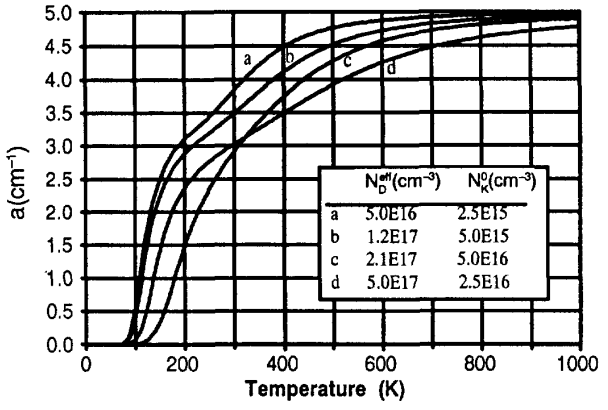

Fig. 12. Calculated carrier removal rate (in low fluence limit) versus temperature for several values of doping and compensation densities.

we take the compensation densities to be 5% of the doping. We assume $A = 5.0\ \text{cm}^{-1}$ in all cases. Note that $a \rightarrow A$ in all cases at high temperatures as expected. Curve c drops to zero faster as the temperature decreases relative to the other curves. This is due to the high compensation level in the lot A devices, which results in a relatively much lower Fermi level at the lower temperatures. Note the structure (shoulders) apparent in all curves but c at low temperature (150 to 200K) and in curves a and b at higher temperature (400–600K). This results from E_F moving down through the two donor levels as the temperature increases. The high temperature (deeper donor level) shoulder is not so apparent in curves c and d because the shoulder occurs at such high temperature that it smeared out. Finally, for the record we note that the RT value of a for the earlier data of ref. 1 (curve c) is $2.9\ \text{cm}^{-1}$.

C. Mobility Degradation

Now armed with a value for A and the calculated a vs T curve, we can infer the dependence of mobility on ϕ from the change in g_m or I_{DSS}, which are proportional to the product $n\mu$ (Eqs. (2) and (3)). I_{DSS} has an additional dependence on N_D^{eff}, but because of the uncertainty associated with the detrapping of the electrons from the deep levels as the temperature is raised, we will use I_{DSS} data only at RT; at higher temperatures we use only g_m data. In Fig. 13 we show the result for the extraction of the mobility parameter β at RT. Here, we plot μ_o/μ_ϕ versus ϕ for several sets of data, which according to Eq. (10) should be a straight line with slope β. The data sets included in Fig. 13 include both g_m and I_{DSS} measurements taken at both the APRF and MUTR facilities; at the MUTR we include data taken both while the reactor was powered and later in time after completion of the irradiation. It is clear that except for one spurious data point, all the data are well fit by a straight line with the slope $1.05 \times 10^{-16}\ \text{cm}^2$, indicating that the mobility would be reduced by a factor of two at a fluence of $1 \times 10^{16}\ \text{cm}^{-2}$. The one spurious data point (I_{DSS}) occurred at the highest fluence point during the powered-up state at the MUTR. This point was traced to an excess current (perhaps a drain leakage current along the surface of the passivation oxide) which disappeared within several minutes after powering down the reactor, resulting in the point immediately above the solid line at the fluence $4.5 \times 10^{15}\ \text{cm}^{-2}$. Again, because of the uncertainties associated with the various measurements that enter the analysis we would ascribe an accuracy no better than about ±25% to the value of β.

Next, we analyze the temperature dependence of the β-parameter, since the simple theory we are using (Eq. (11)) indicates a strong power law temperature dependence. As mentioned above we use only g_m data for this analysis. We also use only APRF irradiation data (except for a single RT MUTR g_m point used simply to indicate consistency of the MUTR data with the APRF data). To eliminate the relatively weak temperature dependence associated with $a(T)$, we define the auxiliary function $\beta'(T) = \{[2A\text{-}a(T_o)]/[2A\text{-}a(T)]\}\beta(T)$. Hence, according to Eq. (11), $\beta'(T) \sim T^{-7/2}$. Figure 14 shows a plot of $\log \beta'$ vs $\log T$ from RT to 300°C. The solid line is simply a straight line of slope −3.5 drawn through the RT APRF point. It obviously provides a good description of the data and points to the validity of the simple theory used here.

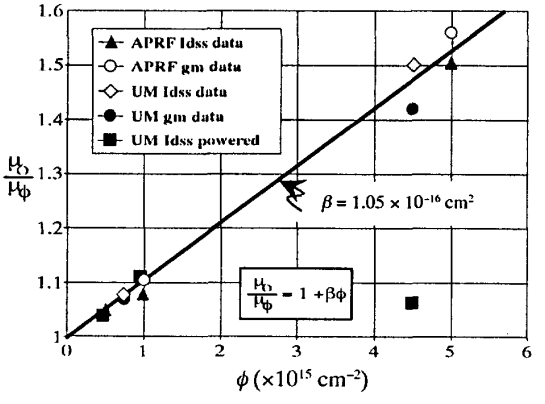

Fig. 13. Extraction of room temperature mobility parameter (b) from g_m and I_{DSS} data as function of neutron fluence.

Finally, to emphasize the strong temperature dependence of the neutron effect on mobility, we show in Fig. 15 calculated curves of mobility versus fluence at several temperatures using Eq. (10), scaling μ_o as T^{-2} from its measured RT value of 320 cm^2/V-s, and using Eq. (11) to scale β from the RT value of 1.05×10^{-16} cm^2 determined in Fig. 13. The upper curve in Fig. 15 shows the result for μ versus ϕ at room temperature. Note that μ drops by about a third of its pre-rad value at a fluence of $\approx 5 \times 10^{15}$ cm^{-2}. The experimental value of g_m at $\phi = 5 \times 10^{15}$ cm^{-2} is degraded to 40% of its pre-rad value of 6.45 mS/mm, with roughly comparable contributions in the reduction coming from carrier removal (28%) and mobility reduction, along with a smaller (≈10%) effect arising from the change in pinchoff voltage (see Eq. (2)). The lower curve in Fig. 15 is the calculated μ versus ϕ curve at 300°C for which β is scaled to 0.08×10^{-16} cm^2. Note that the relative neutron effect on μ is an order of magnitude less at 300°C than at RT. As a result, we attribute the relative neutron effect on g_m almost solely to carrier removal at 300°C, observing also from Fig. 4(a) virtually no change in threshold voltage with ϕ at 300°C. In fact, at 300°C g_m is reduced (Fig. 4(b)) to about 0.76 of its pre-rad value at a fluence of 5×10^{15} cm^{-2}. The calculated reduction due to carrier removal (see Fig. 11) is 21%, which along with an additional 4% effect from mobility is in complete agreement with the experimentally observed reduction. This is the consistency check we alluded to earlier which supports our assertion that the measured RT change in V_{po} provides a good lower bound on the defect introduction rate.

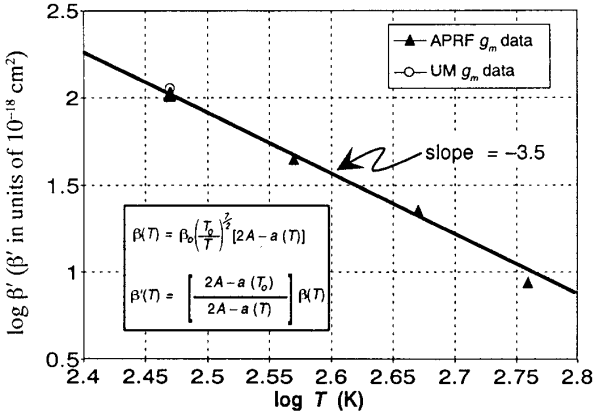

Fig. 14. Log-log plot of auxiliary parameter $b\phi$ versus T, indicating −7/2 power law dependence of mobility parameter with temperature

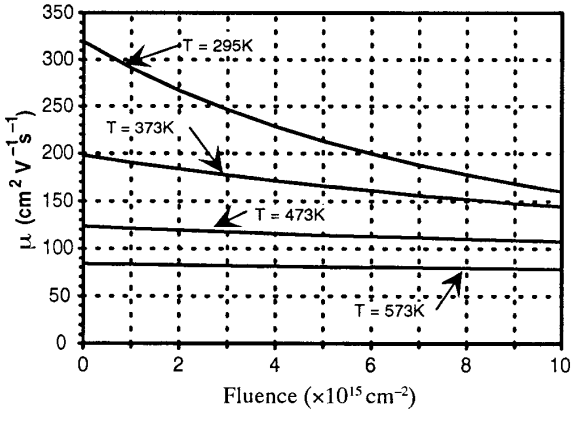

Fig. 15. Calculated carrier mobility versus neutron fluence at four temperatures.

V. Discussion

It is clear from the data reported here that the present SiC JFETs are relatively quite hard to neutron irradiation. For example, from Fig. 4 we observe at a fluence of 1×10^{15} cm^{-2} less than 10-percent reduction in the device parameters over the temperature range studied (RT to 300°C). Even at a fluence of 5×10^{15} cm^{-2}, at 300°C there is only about a 25 % reduction in g_m or I_{DSS}. Furthermore, since at 300°C the neutron effect is essentially due only to carrier removal (with essentially full ionization of the donors being achieved and $a \approx A$ at this temperature), we expect little additional change in the *relative* neutron effect at even higher temperatures—until a sufficiently high temperature is reached that annealing of the neutron-induced damage occurs. (See below for further discussion.)

With these comments in mind, we can easily arrive at some general steps necessary to harden SiC JFETs to higher neutron fluences. For example, if one wanted devices to operate at temperatures 300°C and above to a neutron fluence of 1×10^{16} cm^{-2} (which has been a stated goal for 10-year lifetime space nuclear power applications), then a doping density of 5×10^{17} cm^{-3} would be required, assuming a criterion of 10% maximum reduction in the device electrical parameters and the same defect introduction rate of 5 cm^{-1} as determined here. In fact, we attempted to procure such devices for the present study so that we could experimentally demonstrate 1×10^{16} n/cm^2 hardness. However, in order to keep the threshold voltage reasonable, i.e., to ≤10 V, the channel depth had to be decreased to something less than 150 nm (see Eq. (1)). The first attempt at fabrication of such devices proved unsuccessful. We do not believe this to be any fundamental obstacle, but rather indicative of a yet immature and emerging technology. Thus, actual demonstration of neutron hardness to 1×10^{16} cm^{-2} fluence remains for a further study. (Also, the new devices we tried to obtain were top-gated as opposed to the bottom-gated devices used here. This would have the additional advantage of possibly eliminating the small enhancement effect observed here at low neutron fluence, which we believe is associated with gamma-induced charging of the passivation oxide above the channel in the present (lot B) devices. Even though the effect is one of enhancement, it would still be generally best to eliminate it, because it is basically uncontrollable.)

The question of annealing of the neutron-induced damage arises naturally. The short answer is that we have observed no evidence of any annealing occurring over the temperature range we have studied (RT to 300°C) either in this work or our previous study [1]. The neutron-induced defects appear quite stable in the temperature and time regimes of our measurements. With this said, though, we cannot claim to have conducted any kind of rigorous study of annealing effects. However, our casual obser-

vations are completely consistent with the only comprehensive study of defect annealing after neutron irradiation of n-type 6H-SiC that we have found in the literature—that of a Russian group at the Ioffe Institute [19]. Their samples were single crystals of n-type 6H-SiC with uncompensated donor concentrations between 1×10^{17} and 1×10^{18} cm^{-3}, and their measurements included x-ray diffraction, Hall effect, and optical absorption. They conducted isochronal annealing in the temperature range 200–2600°C after irradiation with reactor neutrons. Their principal conclusions which are pertinent to our work include the following: (1) essentially no annealing occurred below 500°C; (2) the radiation-induced, electrically active gap states annealed in a narrow temperature range above 1000°C; (3) 30–40% of all defects were annealed by 1200°C; (4) complete annealing of the damage occurred by 1700°C for fluences less than 1×10^{18} cm^{-2}; and (5) for larger neutron fluences stable damage existed all the way to 2600°C.

As to the possible energy levels of the neutron-induced gap states, we really cannot say much quantitatively based on the results of this study. What is required to do this is a careful deep-level transient spectroscopy (DLTS) study, which we are currently setting up and hope to carry out on our devices in the near future. What we can say based on the present results is, first, that the induced traps essentially remain fully occupied in the quasi-neutral channel region up to at least 300°C. At this temperature and after irradiation to a fluence of 5×10^{15} cm^{-2}, the calculated Fermi level is 0.30 eV below the conduction band edge (E_c). Therefore, for full occupation the induced levels must lie several kT below this value, putting them at least 0.40 eV below E_c. Second, based on the behavior of the threshold voltage as a function of temperature after irradiation (Fig. 4a), we conclude that in the depletion region the deep traps remain filled with electrons at RT but that at 300°C the trapped electrons are mostly all ejected on the time scale of the measurements (seconds). Based on simple emission time arguments [20], we estimate that the induced trap energy levels lie in the range 0.8 to 1.7 eV below E_c. (Here, we are using the expression $t_e = (g/\sigma_c v_{th} N_c) \exp(E_T/kT)$ for emission time t_e from a trap with energy E_T below E_c, where σ_c is the capture cross section by a Coulomb center and v_{th} is the thermal velocity of a free carrier. For our estimate we are taking $\sigma_c \sim 1 \times 10^{-13}$ cm^2 and setting $t_e = 10$ s.) This energy range is consistent with the conclusion of the Russian group [19] that the electrically active neutron-induced defects were nonradiative recombination centers lying in the midgap region.

Finally, we make a few comments concerning the low fluence enhancement effect that we observed and attributed (see Section II) to positive charging of the passivation oxide above the channel by the gamma dose. We note that such an effect has also been observed in GaAs by Khanna et al [21] and Jorio et al [22]. These workers attributed the effect in their case to a radiation-induced ordering effect in which the nature and distribution of preirradiation defects are changed by the radiation in such a manner as to improve the electronic properties. To support the notion that the low fluence enhancement effect in our case is likely due to a positive charge buildup in the oxide, we note that it occurs at roughly an order of magnitude lower neutron fluence at the MUTR than at the APRF but at approximately the same gamma dose (due to the different ratios of gamma dose to neutron fluence). Also, the effect is most evident at RT, which is consistent with annealing of oxide charge (and interface traps) at higher temperatures. Furthermore, the areal density of the carriers in the channel at RT looking down from the top (Fig. 1) through the channel depth D is $nD = (0.62 \times 10^{17}\text{cm}^{-3})(3.2 \times 10^{-5}$ cm) $\approx 2 \times 10^{12}$ cm^{-2}. This means that to effect a 10% increase in the effective areal carrier density requires a positive oxide charge density of only about 2×10^{11} cm^{-2}, a very plausible charge buildup even at zero applied field across the oxide (though fringing fields between the drain and source regions do exist in the oxide layer). A final point, based on the discussion above on annealing (or lack thereof), is that defects in SiC appear to be essentially immobile at RT. In the end, however, these arguments are all speculative in nature, and further elucidation of the low fluence enhancement effect in the SiC JFETs remains a topic for future study.

VI. Summary

We have presented a more complete analysis of neutron-induced displacement damage effects in n-type 6H-SiC JFETs than previously [1], in which, by folding in new information on the ionization energy structure of the nitrogen donors, we can account for the change in Fermi potential with both temperature and neutron fluence. A better description of carrier removal and mobility reduction is thereby obtained. A value of 5 ± 1 cm^{-1} is found for the fundamental defect introduction rate. The carrier removal rate is temperature dependent, varying from 3.5 cm^{-1} at room temperature, where there is only partial ionization of the N donor atoms, to 4.75 cm^{-1} at 300°C. The relative neutron-induced degradation in mobility is strongly temperature dependent, scaling approximately as $T^{-7/2}$. At RT a fluence of 1×10^{16} cm^{-2} reduces the mobility by a factor of two, but at 300°C the neutron effect is an order of magnitude less.

In conclusion, the results of this study offer further encouragement for the use of SiC devices that must withstand both high-temperature and severe radiation environments, where the use of standard Si and GaAs technologies is limited.

VII. Acknowledgments

We wish to acknowledge partial support of this work by the U.S. Army Space and Strategic Defense Command and the Defense Nuclear Agency. We also wish to thank the staffs of the U.S. Army's Pulsed Reactor Facility at Aberdeen, MD, and the Maryland University Training Reactor at College Park, MD, for their support and assistance in carrying out the irradiations of our devices.

VIII. References

[1] J. M. McGarrity, F. B. McLean, W. M. DeLancey, J. Palmour, C. Carter, J. Edmond, and R. E. Oakley, "Silicon Carbide JFET Radiation Response," *IEEE Trans. Nucl. Sci.* **39**, p. 1974, 1992.

[2] W. Suttrop, G. Pensl, W. J. Choyke, R. Stein, and S. Leibenzeder, "Hall Effect and Infrared Absorption Measurements on Nitrogen Donors in 6H-Silicon Carbide," *J. Appl. Phys.* **72**, p. 3708, 1992.

[3] F. B. McLean, C. W. Tipton, and J. M McGarrity, "Electrical Characterization of n-Channel, 6H-SiC JFETs as a Function of Temperature," in *Proc. 5th Internat. Conf. on Silicon Carbide and Related Materials—1993* (Internat. Inst. Phys. Conf. Series, No. 137), edited by M. Spencer et al, IOP Publishing Ltd., Bristol, England, 1994, p. 507.

[4] H. Kang and R. B. Hilborn, Jr., "Resistivity and Hall Coefficient Measurements on SiC," *Proc. 3rd Internat. Conf. on Silicon Carbide*, Miami Beach, FL, edited by R. C Marshall, J. W. Faust, Jr., and C. E. Ryan, 1973, p. 493.

[5] T. Tachibana, H. S. Kong, Y. C. Wang, and R. F. Davis, "Hall Measurements as a Function of Temperature on Monocrystalline SiC Thin Films," *J. Appl. Phys.* **67**, p. 6375, 1990.

[6] W. J. Choyke, "Optical and Electronic Properties of SiC," in *Physics and Chemistry of Carbides, Nitrides, and Borides*, edited by R. Freer, Kluwer Academic Publishers, Boston, 1989, p. 563.

[7] R. F. Davis, G. Kelner, M. Shur, J. W. Palmour, and J. A. Edmond, "Thin Film Deposition and Microelectronic and Optoelectronic Device Fabrication and Characterization in Monocrystalline Alpha and Beta Silicon Carbide," *Proc. IEEE* **79**, p. 677, 1991.

[8] P. A. Ivanov and V. E. Chelnokov, "Recent Developments in SiC Single-Crystal Electronics," *Semicond. Sci. Technol.* **7**, p. 863, 1992.

[9] W. J. Schaffer, H. S. Kong, G. H. Negley, and J. W. Palmour, "Hall Effect and C-V Measurements on Epitaxial 6H and 4H SiC," in *Proc. 5th Internat. Conf. on Silicon Carbide and Related Materials—1993* (Internat. Inst. Phys. Conf. Series, No. 137), edited by M. Spencer et al, IOP Publishing Ltd., Bristol, England, 1994, p. 155.

[10] C. J Scozzie, C. W. Tipton, W. M. Delancey, J. M. McGarrity, and F. B. McLean, "High Temperature Stressing of SiC JFETs at 300°C," *Proc. 1994 IEEE Internat. Rel. Phys. Symp.*, San Jose, CA, 1994, p. 351.

[11] S. M. Sze, *Physics of Semiconductor Devices*, 2nd Ed., John Wiley, New York, 1981, p. 316 and 27.

[12] J. A. Edmond, D. G. Waltz, S. Brueckner, H-S Kong, J. W. Palmour, and C. H. Carter, Jr., "High Temperature Rectifiers in 6H-Silicon Carbide," *Proc. 1st Internat. High Temp. Elect. Conf.*, Albuquerque, NM, 1991, p. 500.

[13] P. Srichaikul, A.-B. Chen, and W. J. Choyke, "Electronic Band Structures of SiC Calculated from a Hybrid Pseudopotential and Tight-Binding Model," *Amorphous and Crystalline Silicon Carbide IV*, edited by C.Y. Yang, M. M. Rahman, and G. L. Harris, (Springer Proceedings in Physics, Vol. 71), Springer-Verlag, Berlin, 1992, p. 170.

[14] C. H. Park, B-H. Cheong, K-H. Lee, and K. J. Chang, "Structural and Electronic Properties of Cubic, 2H, 4H, and 6H SiC," *Phys. Rev. B* **49**, p. 4485, 1994.

[15] V. A. J. van Lint, T. M. Flanagan, R. E. Leadon, J. A. Naber, and V. C. Rogers, *Mechanisms of Radiation Effects in Electronic Materials*, John Wiley, New York, Vol. 1, 1980, p. 270.

[16] G. C. Messenger and M. S Ash, *The Effects of Radiation on Electronic Systems*, Van Nostrand Reinhold, New York, 1986, p. 157.

[17] H. J. Stein and R. Gereth, "Introduction Rates of Electrically Driven Active Defects in n- and p- Type Silicon by Electron and Neutron Irradiation," *J. Appl. Phys.* **39**, p. 2890, 1968.

[18] A. L. Barry, B. Lehmann, D. Fritsch, and D. Braunig, "Energy Dependence of Electron Damage and Displacement Threshold Energy in 6H Silicon Carbide," *IEEE Trans. Nucl. Sci.* **38**, p. 1111, 1991.

[19] R. N. Kyutt, A. A. Lepneva, G. A. Lomakina, E. N. Mokhov, A. S. Tregubova, M. M. Shcheglov, and G. F. Yuldashev, "Formation of Defects During Annealing of Neutron-Irradiated Silicon Carbide," *Sov. Phys. Solid State* **30**, p. 1500, 1988.

[20] D. K. Schroder, *Semiconductor Material and Device Characterization*, John Wiley, New York, 1990, p. 306.

[21] S. M. Khanna, C Rejeb, A. Jorio, M. Parenteau, C. Carlone, and J. W. Gerdes, Jr., "Electron and Neutron Radiation-Induced Order Effect in Gallium Arsenide," *IEEE Trans. Nucl. Sci.* **40**, p. 1350, 1993.

[22] A. Jorio, M. Parenteau, M. Aubin, C. Carlone, S. M. Khanna, and J. W. Gerdes, Jr., "A Mobility Study of the Radiation Induced Order Effect in Gallium Arsenide," this issue, Dec. 1994.